Brillouin light scattering on Fe/Cr/Fe thin-film sandwiches

P. Kabos, C. E. Patton, M. O. Dima, and D. B. Church
Department of Physics, Colorado State University, Ft. Collins, Colorado 80523

R. L. Stamps and R. E. Camley
Department of Physics, University of Colorado, Colorado Springs, Colorado 80933

(Received 4 November 1993; accepted for publication 8 December 1993)

Brillouin light scattering (BLS) in the backscattering configuration has been used to study the magnetic excitations in epitaxial Fe(38 Å)/Cr(13 Å)/Fe(38 Å) thin-film sandwiches. Spin-wave frequency was measured versus in-plane wave vector **k** and static in-plane magnetic field **H** for both [100] and [110] direction fields and with **k** perpendicular to **H**. The range of applied fields was 50–1500 Oe. The wave-number range was 0.45×10^5–2.3×10^5 rad/cm. The BLS spectra correlate with magnetization versus field profiles and confirm the antiferromagnetic coupling between the Fe layers. Under low-field conditions and near-antiparallel alignment of the Fe layer magnetization vectors, the spin-wave frequencies from the Stokes and anti-Stokes sides of the BLS spectra are different. These frequencies merge at high field. The low-field splitting feature is very sensitive to small differences in thickness for the magnetic layers and indicates a thickness difference of 9%. Matchups between features of the BLS data and magnetization curves were obtained for the following parameters: magnetic layer saturation induction $4\pi M_s=18.6$ kG; cubic anisotropy field $H_A=550$ Oe; in-plane [110] uniaxial anisotropy field $H_U=76$ Oe; antiferromagnetic interlayer exchange coupling field $H_J=120$ Oe. Spin-wave frequency calculations based on these parameters show quantitative agreement with the measurements. The quantitative fits require inclusion in the theory of an iron layer surface anisotropy with an effective surface anisotropy field of 2 kOe.

I. INTRODUCTION

Multilayer thin films and thin-film sandwiches of Fe and Cr have been the subject of intensive study because of the antiferromagnetic interlayer coupling and the large magnetoresistance which has been found for such structures.[1–3] At the same time, Brillouin light scattering (BLS) has proved to be an important experimental tool for the investigation of microwave magnetic excitations in bulk and thin-film magnetic materials in general,[4,5] and in sandwiches and multilayers in particular.[6–19] The BLS work reported for Fe/Cr/Fe structures has focused mainly on the effect of interlayer thickness on the spectra and the determination of the interlayer exchange coupling.[2,18,20–26] There have been no systematic studies of the BLS spectra as a function of field or wave vector. The interplay between the interlayer exchange and various anisotropies in Fe/Cr/Fe sandwich films does lead to a variety of canted magnetization states, magnetization jumps, and saturation effects for different field ranges which show interesting correlations with the ferromagnetic resonance (FMR) response.[27] Soft-mode behavior has also been observed from data on FMR and BLS frequencies versus field for Fe/Cu/Fe sandwiches and multilayer films.[15,19,22] These works suggested that one might be able to observe characteristic field dependencies for the low-order spin-wave modes in Fe/Cr/Fe sandwich films by light scattering. Additionally, it was expected that these modes might show characteristic wave-vector dependencies in the different field ranges corresponding to antiparallel alignment, canting, and parallel alignment which might serve to empirically elucidate the physical nature of these modes according to the surface mode and volume mode schemes used extensively for single layer films.[28,29]

The objective of this work, therefore, was to perform BLS measurements of the field and wave-vector dependencies of the frequencies of the fundamental magnetic excitations in Fe/Cr/Fe thin-film sandwiches with antiferromagnetically coupled magnetic layers, correlate these results with magnetization versus field data on such films, and compare the observed dependencies with theory for low-wave-number spin-wave modes in sandwich films. The measurements were made for the in-plane static magnetic field **H** along the crystallographic [100] and [110] directions, with the in-plane wave vector **k** always perpendicular to **H**.

The mode frequencies are on the order of those expected for magnetostatic wave excitations in thin films with in-plane fields. The field and orientation dependencies of the sandwich film magnetostatic wave mode frequencies reveal interesting correlations with the different magnetization configurations in the high- and low-field regimes. There are distinct effects due to the antiferromagnetic interlayer exchange, the cubic anisotropy, an additional in-plane [110] direction uniaxial anisotropy, a small difference in thickness for the iron layers, and a surface anisotropy. The data have been analyzed on the basis of a full theory for spin waves in two very thin exchange-coupled films developed by Stamps.[30] This theory gives good agreement with the light-scattering data for both [100] and [110] direction fields.

 0021-8979/94/75(7)/3553/11/$6.00 © 1994 American Institute of Physics

Downloaded 26 Dec 2001 to 129.82.140.114. Redistribution subject to AIP license or copyright, see http://ojps.aip.org/japo/japcr.jsp

II. Fe/Cr/Fe FILM PROPERTIES

The Fe/Cr/Fe multilayer films for this work were grown by molecular-beam epitaxy and characterized at the Naval Research Laboratory (NRL). The measurements reported here are for the same epitaxial (100) Fe(38 Å)/Cr(13 Å)/Fe(38 Å) thin-film sandwich used for the vibrating sample magnetometer hysteresis measurements and FMR measurements reported in Ref. 27. The three-layer film sandwich was grown on a (100) GaAs substrate coated with a 2000-Å-thick (100) ZnSe layer. The film was overcoated with a 1000-Å-thick (100) ZnSe layer for symmetry purposes and for protection of the top iron layer. The 13 Å Cr layer thickness resulted in a moderate antiferromagnetic coupling[2,22] between the two iron layers, as documented in Ref. 27.

Such films may be characterized in terms of the usual [100] easy direction cubic magnetocrystalline anisotropy characteristic of iron, a small amount of uniaxial anisotropy along one in-plane [110] easy axis, and antiferromagnetic interlayer exchange coupling. For a sandwich film with single-domain in-plane magnetized magnetic layers of thicknesses d_1 and d_2 and magnetization vectors $\mathbf{M}_1$ and $\mathbf{M}_2$, respectively, one may write the film energy density U per unit area as

$$\frac{U}{M_s}=d_1\left(H\cos(\theta-\phi_1)+\frac{1}{8}H_A\sin^2(2\phi_1)-\frac{1}{4}H_U\sin(2\phi_1)\right)$$
$$+d_2\left(H\cos(\theta-\phi_2)+\frac{1}{8}H_A\sin^2(2\phi_2)\right.$$
$$\left.-\frac{1}{4}H_U\sin(2\phi_2)\right)+(d_1+d_2)H_J\cos(\phi_1-\phi_2). \quad (1)$$

In the above, M_s is the saturation magnetization for the iron. The angles ϕ_1 and ϕ_2 denote the respective angles between the $\mathbf{M}_1$ and $\mathbf{M}_2$ vectors and one specific in-plane [100] direction. The angle θ denotes the angle between the applied in-plane magnetic field H and this [100] direction. The field parameters H_A and H_U characterize the cubic and uniaxial anisotropies indicated above. In terms of the usual first-order cubic anisotropy and uniaxial anisotropy energy density parameters K_1 and K_u, these fields may be written as $H_A=2K_1/M_s$ and $H_U=2K_u/M_s$, respectively. The antiferromagnetic coupling between the iron layers is specified in terms of the exchange field H_J. Positive H_J gives a minimum energy for $\mathbf{M}_1$ and $\mathbf{M}_2$ antiparallel. This interlayer exchange coupling is often expressed in terms of a volume exchange energy density parameter $J=M_s H_J$ or a surface exchange energy density parameter $A_{12}=J(d_1+d_2)/2$. Equation (1) is used to evaluate static equilibrium values of ϕ_1 and ϕ_2 as a function of H for the model magnetization curve calculations in Sec. IV and for the theoretical spin-wave frequency calculations in Sec. V. The magnetocrystalline anisotropy easy [100] direction in-plane field case corresponds to $\theta=0$. Because of the uniaxial anisotropy, the two in-plane [110] field directions are inequivalent. The $\theta=+45°$ case corresponds to the uniaxial easy axis and for $\theta=-45°$ the field is perpendicular to this easy axis. Nominal values for the magnetic parameters for the sandwich from Ref. 27 are $4\pi M_s=18.6$ kG, $H_A=500$ Oe, $H_U=76$ Oe, and $H_J=150$ Oe.

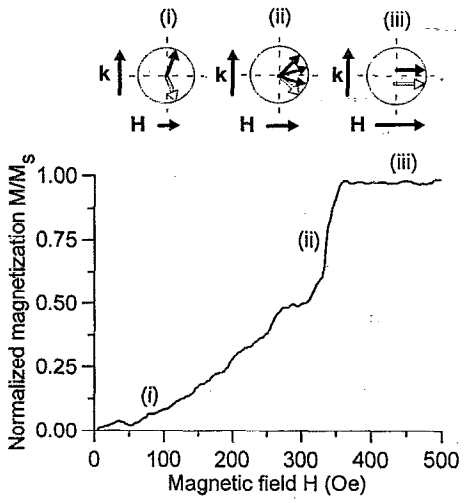

FIG. 1. Measured [100] direction magnetization curve of the normalized magnetization M/M_s vs magnetic field H for the Fe/Cr/Fe sandwich film. The top diagram shows schematic magnetization configurations for the two Fe layers in the three indicated regions of the magnetization curve. The vector H denotes the field and k denotes the Brillouin light-scattering spin-wave wave vector.

Figures 1 and 2 show measured first quadrant magnetization curves of reduced magnetization M/M_s versus in-plane magnetic field H for the sandwich for in-plane [100] direction and [110] direction fields, respectively. The measurements were obtained at NRL by vibrating sample magnetometry. The curve in Fig. 2 is from Ref. 27. The diagram at the top of the figures shows in schematic form the orientations of the two Fe layer magnetization vectors as-

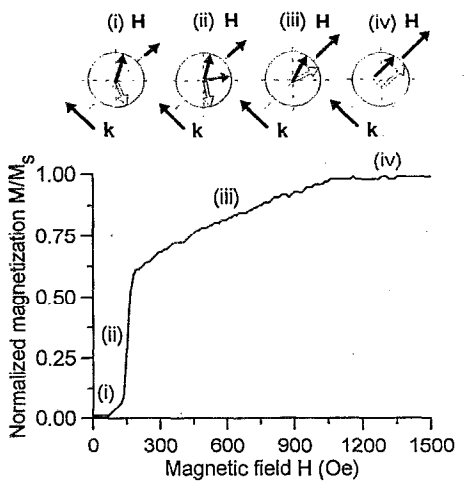

FIG. 2. Measured [110] direction magnetization curve of the normalized magnetization M/M_s vs magnetic field H for the Fe/Cr/Fe sandwich film (from Ref. 27). The top diagram shows schematic magnetization configurations for the two Fe layers in the four indicated regions of the magnetization curve. The vector H denotes the field and k denotes the Brillouin light-scattering spin-wave wave vector.

Downloaded 26 Dec 2001 to 129.82.140.114. Redistribution subject to AIP license or copyright, see http://ojps.aip.org/japo/japcr.jsp

sociated with different regions of the curve. The dashed lines on the individual film circles show the [100] directions. The solid arrows represents the magnetization vector $\mathbf{M}_1$ for one layer and the open arrows the magnetization vector $\mathbf{M}_2$ for the other layer. The shadowed arrows indicate jumps in the magnetic moments. The direction and size of the field $\mathbf{H}$ is indicated on each diagram as well. The diagrams also show the Brillouin light-scattering spin-wave wave vector $\mathbf{k}$.

The magnetization curve in Fig. 1 shows three distinct regions, labeled (i), (ii), and (iii). In the low-field region (i), 0–350 Oe or so, the change in magnetization with field is more or less reversible. Here, the antiferromagnetic coupling dominates to keep the vectors nearly antiparallel and the small deviation from the antiparallel state is produced by the field. The corresponding magnetization configuration is shown by insert (i). In the intermediate field region (ii), 350–375 Oe or so, the field is sufficient to cause the magnetization vectors to flip to a more nearly parallel configuration. Here, the effect of field dominates to keep the vectors nearly parallel and the antiferromagnetic coupling leads to the small deviation from parallel alignment. This flip, shown in insert (ii), causes the rapid increase in M labeled as (ii) in Fig. 1. Finally, in region (iii), the field is sufficient to align the vectors parallel and the magnetization curve is saturated.

In principle, the effect of the small in-plane [110] axis uniaxial anisotropy should show up as a small plateau which decorates the region (ii) jump. Such a plateau does not show up in the magnetization data of Fig. 1. As will be evident from the BLS data, such a plateau will be well resolved in the light scattering measurements. This plateau will constitute an important aspect of the experimental results.

The diagram at the top of Fig. 1 also shows the wave vector $\mathbf{k}$ for the spin-wave excitations measured by the BLS technique. It is important to note that this $\mathbf{k}$ vector is more or less collinear with the magnetization vectors in region (i) and perpendicular to these vectors in region (iii). In the single-layer situation, backward volume wave magnetostatic backward volume modes are expected when the vector magnetization $\mathbf{M}_s$ and $\mathbf{k}$ are collinear. Magnetostatic surface wave modes are expected when $\mathbf{M}_s$ and $\mathbf{k}$ are perpendicular. This change in the iron layer magnetization directions relative to $\mathbf{k}$ leads to observable changes in the spin-wave frequency versus wave-number character which are connected with surface mode and volume mode considerations.

Figure 2 shows a measured in-plane [110] direction magnetization versus field curve and companion insert diagram for the sandwich. The curve follows the data in Fig. 3 of Ref. 27. Note the 45° rotation of the field direction relative to the insert diagram in Fig. 1. The curve and diagram are for one of the [110] field cases only. The basic processes here are the same as for the [100] direction except that the initial magnetization state is with antiparallel Fe layer magnetization vectors at 45° and 135° to the field direction, respectively. There are now four regions. In region (i), up to about 170 Oe, one has small rotations for both $\mathbf{M}$ vectors away from their antiparallel orientation, as before. Region (ii) corresponds to a jump at about 170 Oe for one of the $\mathbf{M}$ vectors to a position closer to the field direction, as shown by the shaded arrow in insert (ii). Region (iii), from 170 up to about 1100 Oe, consists of a gradual rotation of both magnetization vectors with increasing field. Region (iv), for fields above 1100 Oe, corresponds to saturation, with the iron layer magnetization vectors both aligned with the field. The magnetization processes summarized above follow the basic arguments given in Ref. 27. Note the BLS $\mathbf{k}$ vectors indicated in the diagram at the top of Fig. 2. For this [110] direction field situation, the $\mathbf{M}$ vectors are never strictly collinear with or perpendicular to $\mathbf{k}$.

Because of the uniaxial anisotropy with an easy axis along one of the in-plane [110] directions, one would expect the magnetization curves for the two in-plane [110] directions to be slightly different. This point will be considered below, in connection with the BLS data. The basic shapes for both curves are as shown in Fig. 2.

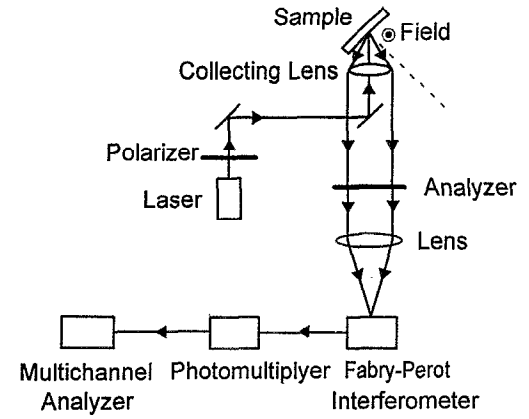

FIG. 3. Schematic diagram showing the backscattering geometry and spectrometer instrumentation for the Brillouin light-scattering detection of thermal magnetic excitations in Fe/Cr/Fe thin-film sandwiches.

III. BRILLOUIN LIGHT SCATTERING

The Brillouin light-scattering technique for the measurement of magnetic excitations is described in Refs. 4 and 5. Figure 3 shows the experimental setup for BLS measurements in the backscattering configuration. The magnetic field is applied in the film plane and perpendicular to the plane of incidence of the incident light. Linearly polarized laser light at some nonzero angle of incidence relative to the film normal is focused on the film. Thermally excited spin waves in the film interact with the incident light to produce scattered light which is upshifted or downshifted from the laser light frequency. The light is then analyzed with a multipass-tandem Fabry–Pérot interferometer, detected by a high-sensitivity low-dark-count photomultiplier tube, and recorded by means of photon counting system and a multichannel analyzer. The magnetic field was produced with a small iron yoke electromagnet with a maximum field of 4900 Oe. The light source was a single-mode-stabilized argon laser operated at a

Downloaded 26 Dec 2001 to 129.82.140.114. Redistribution subject to AIP license or copyright, see http://ojps.aip.org/japo/japcr.jsp

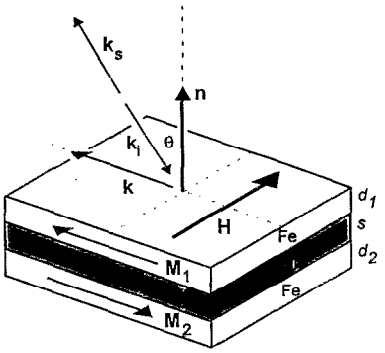

FIG. 4. Backscattering geometry for the Brillouin light-scattering experiment on sandwich films.

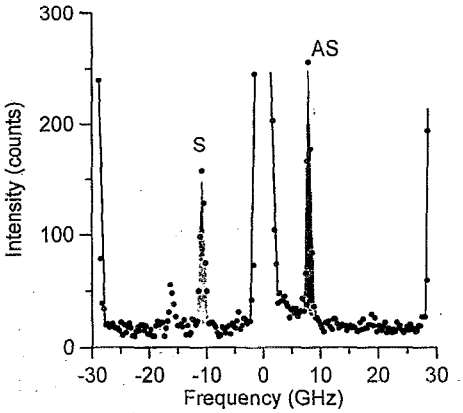

FIG. 5. Brillouin light-scattering spectra for magnetic excitations in the Fe/Cr/Fe sandwich film. The free spectral range of the Fabry–Pérot interferometer was 30 GHz. An in-plane static magnetic field of 72 Oe was applied in the [100] direction. The angle of incidence was 35° and the in-plane spin-wave wave number k was 1.48×10^5 rad/cm.

wavelength λ of 488 nm. All measurements were carried out at room temperature. The laser power incident on the sample was typically 50 mW, low enough to avoid sample heating effects. The Fabry–Pérot interferometer was a Sandercock three-times-two actively stabilized multipass-tandem system with vibration isolation.[31] The contrast and finesse parameters of the system were 10^{12} and 40, respectively. The photon counting system utilized an EMI9863A/100 photomultiplier tube with about 15% quantum efficiency at 488 nm and a dark count below 1/3 count per s.

The backscattering geometry for the film is shown in more detail in Fig. 4. The static magnetic field **H** is applied in the plane of the sandwich and perpendicular to the plane of incidence defined by the surface normal **n** and the incident and scattered light wave vectors $\mathbf{k}_i$ and $\mathbf{k}_s$. The angle of incidence is shown by θ. The individual iron layers have thicknesses d_1 and d_2, and the Cr layer thickness is denoted by s. The magnetizations in the two iron layers, $\mathbf{M}_1$ and $\mathbf{M}_2$, are shown by antiparallel arrows which are both perpendicular to **H**. This corresponds to the [100] direction field case in Fig. 1 in the $\mathbf{H}=0$ limit. For the [110] direction field case, the iron layer magnetizations in the $\mathbf{H}=0$ limit would be at 45° and 135° to the **H** vector in Fig. 4.

For thin metal films and surfaces, only the in-plane spin-wave wave vector contributes to the scattering from lowest-order modes.[19,32] This in-plane wave vector is shown as **k** in Fig. 4. The frequencies of the scattered spin waves are typically in the GHz range, much less than the laser frequency. In this approximation, the light wave numbers $|\mathbf{k}_i|$ and $|\mathbf{k}_s|$ are very nearly equal. If the average index of refraction of the film sandwich is taken as unity and momentum conservation is applied to in-plane wave-vector components only, one obtains the spin-wave wave number k as

$$k=2|\mathbf{k}_i|\sin\theta, \tag{2}$$

where $|\mathbf{k}_i|=2\pi/\lambda$ is the wave number of the incident laser light. The **k** vector shown in Fig. 4 is for the destruction of a magnon and an increase in the frequency of the scattered light. This corresponds to anti-Stokes scattering. For magnon creation, which corresponds to Stokes scattering and a decrease in the frequency of the scattered light, the **k** vector would be in the opposite direction.

The constraints of light collection and sample placement in the magnet gap limited the scattering angles available to the range $10°<\theta<65°$. From Eq. (1), this range of θ values yields spin-wave wave numbers in the range 0.45×10^5 rad/cm $<k<2.3\times10^5$ rad/cm. The lens collection angle was about 33°, which corresponds to a spread in the in-plane wave number of $0–1.15\times10^5$ rad/cm at $k=0.45\times10^5$ rad/cm and $1.93\times10^5–2.57\times10^5$ rad/cm at $k=2.3\times10^5$ rad/cm.

In the theory of magnetostatic waves for thin films[28] and sandwiches,[30] the basic wave-number parameters which enter most of the formulas are dimensionless reduced wave numbers given by kd and ks. In the present case, the film sandwich of interest has individual iron layers of nominal thickness $d=38$ Å and an intermediate chromium layer of thickness $s=13$ Å. The range of reduced wave numbers for the scattering geometry specified above is then given by $0.017<kd<0.087$ and the corresponding range of reduced wave numbers related to the interlayer thickness s is $0.0058<ks<0.0298$. These kd and ks values are all well below unity. This is an important consideration in the analysis and discussion presented later.

A typical Brillouin spectrum of scattering intensity versus frequency shift is shown in Fig. 5. These particular data are for a [100] direction applied magnetic field of 72 Oe and an angle of incidence $\theta=35°$. This θ value corresponds to a wave number $k=1.48\times10^5$ rad/cm. The Fabry–Pérot free spectral range was 30 GHz. The large central peak at zero frequency shift and the two large side peaks at ±30 GHz are the first- and second-order elastic Rayleigh peaks corresponding to scattered photons at the laser frequency. The spin-wave signals are shown by the upshifted anti-Stokes (AS) peak at about +8 GHz and the

Downloaded 26 Dec 2001 to 129.82.140.114. Redistribution subject to AIP license or copyright, see http://ojps.aip.org/japo/japcr.jsp

downshifted Stokes (S) peak at approximately -11 GHz. As indicated above, the upshifted AS peak corresponds to the destruction of a magnon at frequency $\omega=8$ GHz and an increase in the light frequency. The downshifted S peak corresponds to the creation of a magnon at $\omega=11$ GHz and a decrease in the light frequency. The Stokes and anti-Stokes peaks are at different frequencies. For fields above about 100 Oe, the Stokes and anti-Stokes frequencies come together.

IV. EXPERIMENTAL RESULTS AND MAGNETIZATION CURVE CONNECTIONS

For a more complete characterization of the magnetic excitations in the Fe/Cr/Fe sandwich, two sets of experiments were performed. In the first set of experiments, the BLS frequencies were measured at fixed scattering angle and fixed wave number as a function of the magnitude of the in-plane applied external static magnetic field H. These measurements were done with the field **H** along (a) an iron layer in-plane [100] direction and (b) the two iron layer in-plane [110] directions. The objective of these measurements was to examine possible correlations between the BLS frequencies and the magnetization curve characteristics described above. In the second set of experiments, the scattering angle was varied and the BLS frequencies were measured versus the in-plane wave number k in order to obtain actual dispersion curves for the fundamental magnetic excitations in these Fe/Cr/Fe sandwiches. These frequency versus wave number measurements were also carried out for both [100] and [110] direction fields.

Figure 6 shows the results of the measurements for Stokes and anti-Stokes BLS frequency versus in-plane static field H for (a) the [100] direction field case and (b) the two [110] direction field cases. The individual spectra for the frequency measurements were essentially as shown in Fig. 5. The angle of incidence θ was held at 35° for all the measurements, corresponding to $k=1.48\times10^5$ rad/cm and $kd=0.056$. The diamond symbols indicate the measured AS mode frequencies and the circles indicate the S mode frequencies. The solid and open symbols in Fig. 6(b) are for the two different in-plane [110] field directions along and perpendicular to the uniaxial easy axis, respectively. The dashed and solid lines show theoretical curves. The dashed lines show the calculated Damon–Eshbach (DE) surface mode frequencies versus field for a double-thickness 76 Å iron layer with $\mathbf{M}_s$ aligned with **H** and perpendicular to **k**. The solid lines show the results of calculations for the applicable sandwich film spin-wave mode frequencies from the theory of Stamps.[30] The theoretical curves in Fig. 6(b) are for the [110] uniaxial hard in-plane direction field case only. These calculated curves and their relation to the data are discussed in Sec. V.

The data in Fig. 6 show clear correlations with the magnetization curves and processes shown in Figs. 1 and 2. Consider first the in-plane [100] field direction BLS data in Fig. 6(a). The large overall 10 GHz frequency jump at $H\approx250$–300 Oe corresponds to the region (ii) jump in magnetization shown in Fig. 1 at about 350 Oe. The slowly increasing frequency at higher fields is associated with the

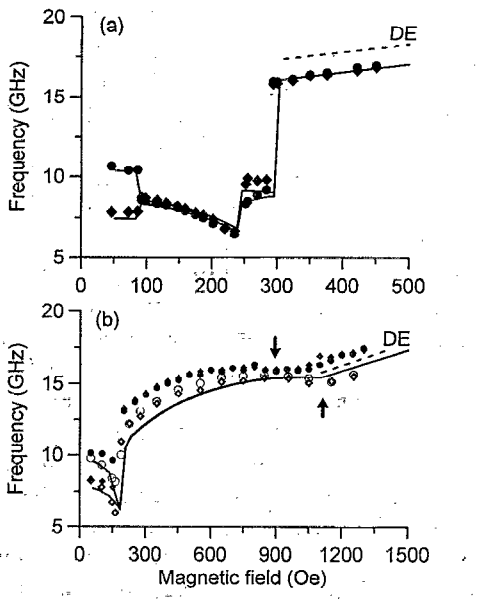

FIG. 6. BLS frequency vs in-plane field for the sandwich film with (a) an in-plane [100] field direction and (b) the two in-plane [110] field directions. The angle of incidence was 35° and the in-plane wave number was 1.48×10^5 rad/cm. The circle and diamond data points are for the Stokes and anti-Stokes spin-wave peaks in the Brillouin light-scattering spectra, respectively. The open and solid symbols in (b) are for the in-plane [110] uniaxial easy axis and uniaxial hard direction field cases, respectively. The dashed lines show calculated frequencies for the Damon–Eshbach surface mode in a double-thickness 76 Å iron layer. The solid lines show calculated frequencies from the theory of Stamps. The calculated lines in (b) are for the [110] uniaxial hard in-plane direction field case only.

spin-wave mode for the region (iii) saturated film state. The rate of increase in this regime is about 4.8 MHz per Oe, which is in good agreement with 4.87 MHz/Oe from the single-slab DE theory for spin-wave modes in a saturated film and 4.75 MHz/Oe from the full theory. In addition to these features, the BLS data for fields below 300 Oe show considerable structure. This structure will be considered shortly.

Similar comments apply to the BLS data in Fig. 6(b) for the two in-plane [110] direction field cases. The solid symbols are for fields in the in-plane [110] direction parallel to the uniaxial anisotropy easy axis. The open symbols are for fields along the in-plane [110] direction perpendicular to this uniaxial easy axis. Although the frequency and field shifts between these two sets of data are significant, the shapes of responses in both cases reflect the basic magnetization processes depicted in Fig. 2. At low field, the Stokes and anti-Stokes frequencies are separated by 2 GHz or so and decrease with field. This behavior corresponds to the region (i) part of the magnetization curve in Fig. 2. Both BLS frequencies show a sharp decrease and then a jump by about 5 GHz at $H\approx200$ Oe. This behavior corresponds to the region (ii) flip in the magnetization vector for one layer at $H\approx170$ Oe shown in Fig. 2. The sharp decrease in the BLS frequencies at the flip point is a manifestation of soft-mode behavior. Above this flip point, the Stokes and anti-Stokes frequencies merge for both data sets, increase smoothly with field, show a gradual turnover

Downloaded 26 Dec 2001 to 129.82.140.114. Redistribution subject to AIP license or copyright, see http://ojps.aip.org/japo/japcr.jsp

to shallow minima near 975 and 1125 Oe, and then increase again with field. The responses in the 200–1000 Oe field range correspond to the region (iii) portion of the magnetization curve in Fig. 2. The shallow minima at $H \approx 975$ Oe for the [110] easy axis data and at $H \approx 1125$ Oe for the [110] hard axis data represent weak soft-mode behavior as the individual layer magnetization vectors saturate in the direction of the field. The increases with field above $H \approx 1200$ Oe correspond to the region (iv) saturated portion of the magnetization curve in Fig. 2.

As just indicated, the shifts between the two sets of data in Fig. 6(b) for the in-plane [110] easy axis direction and [110] hard in-plane direction field cases are significant. The lateral shift of 150 Oe between these two sets of data for fields above the jump at 170 Oe is equal to $2H_U$. The jump itself, due mainly to the competition between the antiferromagnetic interlayer exchange and the cubic anisotropy, is not shifted significantly. The spin-wave frequencies for the [110] easy axis case are higher than the [110] hard direction frequencies by about 1.5 GHz. This is also consistent with the effect of the uniaxial anisotropy and $H_U \approx 76$ Oe. The data in Fig. 6(b) clearly demonstrate the effect of the small uniaxial anisotropy on the spin-wave frequencies.

Return now to the easy direction field BLS data in Fig. 6(a) and the additional features in the data for fields below 300 Oe or so. Two such features are evident. First, for fields below about 90 Oe, the S and AS mode frequencies show a splitting of about 3 GHz. Second, the region (ii) jump in frequency which separates the region (i) rotation and the region (iii) saturation is seen to occur in two stages, with a relatively small 2–3 GHz jump at $H \approx 250$ Oe, a 50-Oe-wide plateau at 7–9 GHz for which the S and AS frequencies show a small splitting, and then a larger jump by about 7–8 GHz at $H \approx 300$ Oe to connect with region (iii). Neither of these features would be expected from the data or the simple magnetization processes depicted in Fig. 1. Their presence in the BLS data demonstrates the power of the light-scattering technique in detecting aspects of the magnetization response not always evident from magnetization data.

Based on model magnetization curves for the exchange coupled magnetic layers in the sandwich film, these features can be explained by two effects, one connected with a small but significant difference in thicknesses for the two magnetic layers and one connected with the in-plane [110] easy axis uniaxial anisotropy. Figure 7 shows three graphs of calculated normalized magnetization M/M_s versus field H responses which demonstrate the effect of various film parameters on the magnetization versus field response and, indirectly, on the BLS frequency versus field response as well. These curves were obtained by stepping the field H and determining the orientations of the two iron layer magnetization vectors $\mathbf{M}_1$ and $\mathbf{M}_2$ which minimize the energy U in Eq. (1) at each field point. All the curves shown are based on $4\pi M_s = 18.6$ kG, $H_A = 550$ Oe, and $H_U = 76$ Oe. The curves in Figs. 7(a) and 7(b) are for the [100] direction field case with $\theta = 0°$. The dashed and solid curves in Fig. 7(c) are for the in-plane [110] uniaxial easy axis direction and [110] uniaxial hard in-plane direction field cases, with $\theta = +45°$ and $\theta = -45°$, respectively.

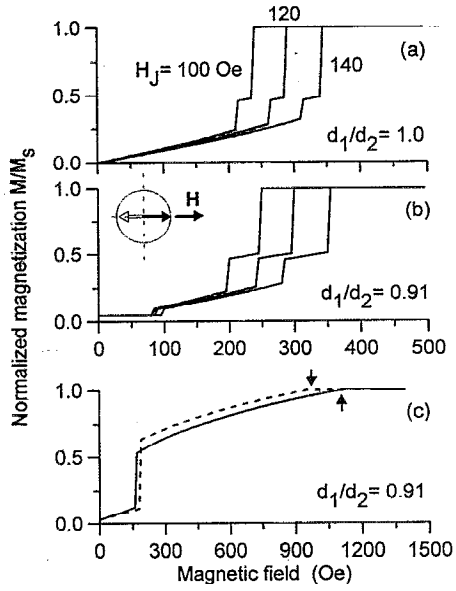

FIG. 7. Calculated curves of the normalized magnetization M/M_s vs in-plane field for an Fe/Cr/Fe sandwich film with an iron layer saturation induction $4\pi M_s = 18.6$ kG, cubic anisotropy field $H_A = 550$ Oe, and uniaxial anisotropy field $H_U = 76$ Oe. The curves in (a) and (b) are for an in-plane [100] direction field. The curves in (a) are based on equal thickness iron layers and values of the effective interlayer exchange coupling field H_J as indicated. The curves in (b) are for the same H_J values as in (a) but with a d_1/d_2 thickness ratio of 0.91 for two iron layers as indicated. The curves in (c) are for $H_J = 120$ Oe and $d_1/d_2 = 0.91$. In (c), the dashed line is for the in-plane [110] uniaxial easy axis direction field case and the solid line is for the [110] uniaxial hard in-plane direction field case.

For Fig. 7(a), the iron layers were taken to be the same thickness and the three curves shown were obtained for the different values of the interlayer effective exchange field H_J as indicated. The curves in Fig. 7(b) are for these same three values of H_J but with a d_1/d_2 thickness ratio of 0.91. The [110] direction curves in Fig. 7(c) are for $H_J = 120$ Oe and $d_1/d_2 = 0.91$. The magnetic parameters are close to the nominal values from Ref. 27 listed in Sec. II. These refined values, however, give a consistent match between all of the observed features in the BLS data and magnetization curve responses. As is shown in Sec. V, these values also yield theoretical curves which quantitatively match the BLS data.

Consider first the results in Fig. 7(a). All curves show the initial steady increase in M/M_s with H associated with the region (i) rotation in Fig. 1. The region (ii) jump to saturation is controlled by H_A and H_J. The jump moves to higher and higher fields as H_J is increased. The plateau in the middle of the jump is controlled by H_U. Note that the width of the plateau is somewhat smaller than indicated by the BLS data in Fig. 6(a) and that the curves show no special feature at lower fields which might connect with the Stokes–anti-Stokes frequency splitting below $H = 90$ Oe.

One possible origin of the low-field feature in Fig. 6(a) is in a small thickness difference for the two iron layers.

Downloaded 26 Dec 2001 to 129.82.140.114. Redistribution subject to AIP license or copyright, see http://ojps.aip.org/japo/japcr.jsp

The effect of such a difference on the magnetization response was found to be significant. The result is shown in Fig. 7(b). The effect of changing the d_1/d_2 thickness ratio from unity to 0.91 causes the net magnetization to remain small and constant up to a field of 80–90 Oe or so. In this low-field regime, the magnetization of the thicker layer is aligned with the field and the magnetization of the thinner layer is opposite to the field. The insert diagram in Fig. 7(b) shows this low-field magnetization configuration. The region (i) rotation process with the $\mathbf{M}_1$ and $\mathbf{M}_2$ vectors perpendicular to the field $\mathbf{H}$, therefore, is inhibited until the field exceeds about 90 Oe. As will become clear from the calculations in Sec. V, this effect is also the origin of the Stokes–anti-Stokes splitting feature in Fig. 6(a) below $H=90$ Oe. The curves in Fig. 7(b) also show that this small difference in thickness for the two iron layers has a significant effect on the plateau which decorates the region (ii) jump. The effect in region (ii) is to widen the plateau width. From the curves in Fig. 7(b), it is clear that the combination of parameters $4\pi M_s=18.6$ kG, $H_A=550$ Oe, $H_U=76$ Oe, $H_J=120$ Oe, and $d_1/d_2=0.91$ yield a calculated [100] easy direction magnetization field response with features which match the features in the corresponding easy direction field BLS spin-wave frequency measurements.

The low-field jump in Fig. 7(b) is extremely sensitive to small changes in the d_1/d_2 ratio. A d_1/d_2 ratio of 0.91 positions the middle $H_J=120$ Oe curve so that all jumps closely match the corresponding features in the BLS data in Fig. 6(a). Even small changes in the d_1/d_2 to 0.90 or 0.92 move the initial jump away from the position of the S-AS splitting feature in Fig. 6(a) at $H=90$ Oe by a significant amount. The S-As splitting feature in the BLS data appears to provide a way to discern very small differences in the magnetic layer thicknesses for antiferromagnetically coupled sandwich films.

Figure 7(c) shows calculated magnetization curves for the two different in-plane [110] directions for the same parameters as listed above. As already shown, these directions are not strictly equivalent because of the uniaxial anisotropy. For fields above the flip point at $H\simeq 170$ Oe, the curves are shifted laterally relative to each other by $2H_U$. The four regions for each curve correspond to the processes discussed in connection with Fig. 2. The field points which separate the four regions match quantitatively the features evident from the BLS data in Fig. 6(b).

The BLS frequency versus field measurements in Figs. 6(a) and 6(b) and the correlation of the features of those data with the model magnetization curves in Figs. 7(b) and 7(c) constitute the main experimental result of this work. It is clear that careful measurements of the Stokes and anti-Stokes frequencies versus field, particularly at low field, constitute a very powerful tool to probe the magnetization processes for thin sandwich films with antiferromagnetically coupled magnetic layers. In particular, the low-field Stokes–anti-Stokes splitting, the exchange jump, and the uniaxial plateau represent well-defined, characteristic features which make it possible to determine accurately and consistently the uniaxial anisotropy, cubic anisotropy, exchange coupling, and magnetic layer thickness ratio.

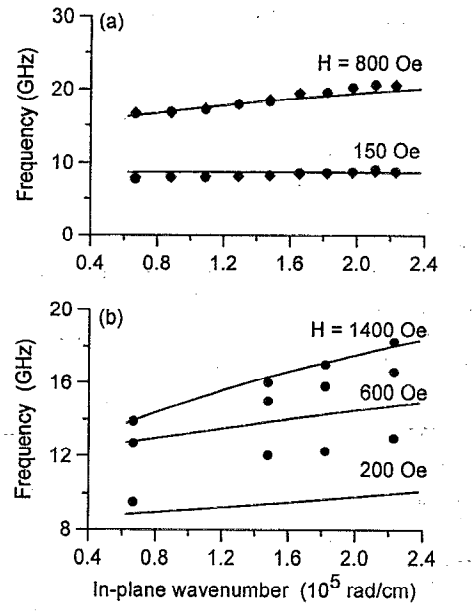

FIG. 8. Brillouin light-scattering (BLS) spin-wave frequency vs in-plane wave number for different values of the in-plane field H for (a) [100] direction fields and (b) [110] uniaxial hard in-plane direction fields. The circle and diamond data points in (a) denote data for the Stokes and anti-Stokes BLS frequencies, respectively. The data in (b) are for the Stokes frequencies only. The solid lines show calculated curves.

Finally, turn to the second set of experiments in which the scattering angle was varied and the BLS spin-wave frequency was measured versus in-plane wave number. The results are summarized in Figs. 8 and 9. Figure 8 shows data on measured BLS frequency versus wave number for different values of the in-plane field $\mathbf{H}$ applied in (a) the [100] direction and (b) the [110] uniaxial hard

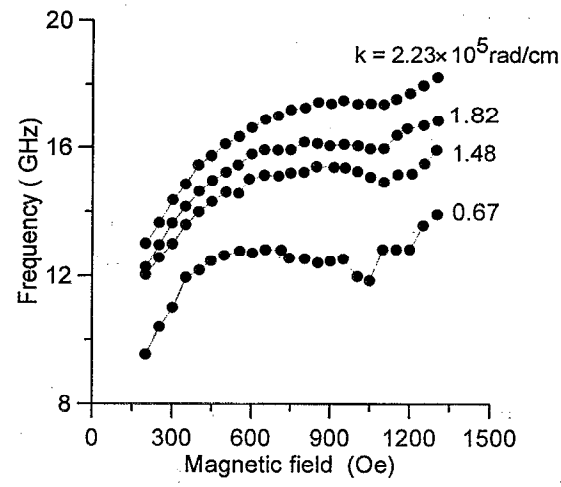

FIG. 9. Brillouin light-scattering (BLS) spin-wave frequency vs [110] uniaxial hard in-plane direction field for different values of the in-plane wave number k. The data are for the Stokes frequencies only.

Downloaded 26 Dec 2001 to 129.82.140.114. Redistribution subject to AIP license or copyright, see http://ojps.aip.org/japo/japcr.jsp

in-plane direction. The solid lines show corresponding results from theory.

Figure 8(a) shows results for one low field, $H=150$ Oe, just above the splitting region, and for one higher field, $H=800$ Oe, which corresponds to saturation. The Stokes and anti-Stokes frequencies are shown by the circles and diamonds, as before. In both cases, the Stokes and anti-Stokes frequencies are nearly equal, as for these same field values in Fig. 6(a), and the increases in frequency with wave number are more or less linear. For the low-field case, the BLS frequencies show a very weak increase with wave number. Here, the fitted slope is about 9 kHz cm/rad. For the high-field case, there is a more rapid increase in the spin-wave frequency with k. The fitted slope for those data is about 29 kHz cm/rad.

The linear k dependencies are consistent with basic Damon–Eshbach theory in the limit $kd \ll 1$. As indicated in Sec. III, this condition is well satisfied for the present measurements. The different slopes for the low- and high-field cases in Fig. 8(a) are also noteworthy. Recall that for low easy direction fields, the iron layer magnetization vectors $\mathbf{M}_1$ and $\mathbf{M}_2$ are nearly antiparallel, approximately perpendicular to the field $\mathbf{H}$, and more or less collinear with the in-plane magnon wave vector $\mathbf{k}$. In the case of single-layer magnetic films, this geometry corresponds to magnetostatic backward volume wave modes and a dispersion curve of ω vs k with a small, negative slope. For high fields and a saturated film with $\mathbf{M}_1$ and $\mathbf{M}_2$ both aligned with $\mathbf{H}$, $\mathbf{k}$ is perpendicular to $\mathbf{M}_1$ and $\mathbf{M}_2$. For single layers, this geometry corresponds to Damon–Eshbach magnetostatic surface modes and a dispersion curve with a positive slope. The sandwich structure shows this basic Damon–Eshbach trend, with a small slope for the low-field case and a larger slope for the high-field case. The small but positive slope for the low-field case indicates that the mode is a surface mode close to the critical angle. At $H=150$ Oe, the angle between $\mathbf{M}_1$ or $\mathbf{M}_2$ and $\mathbf{k}$ is about 8°. The corresponding critical angle in Damon–Eshbach theory is about 11°. From a more quantitative perspective, the full theory for the Fe/Cr/Fe sandwich and parameters listed above yields the solid lines shown in the figure. These lines are in very good agreement with the data.

Figure 8(b) shows results for three different values of the field applied in the [110] uniaxial hard in-plane direction. Only the Stokes data are shown. As is evident from Fig. 6(b), the Stokes and anti-Stokes spin-wave frequencies are the same for hard direction fields above 150 Oe. The lowest-field value, $H=200$ Oe, corresponds to a point just after the region (ii) jump to a region (iii) configuration with the $\mathbf{M}_1$ and $\mathbf{M}_2$ vectors more or less symmetric relative to the field $\mathbf{H}$. The middle-field value, $H=600$ Oe, is in the middle of region (iii), with a decreased angle between the $\mathbf{M}_1$ and $\mathbf{M}_2$ vectors. The highest-field value, $H=1400$ Oe, is well above saturation, with $\mathbf{M}_1$ and $\mathbf{M}_2$ parallel. The BLS frequencies in Fig. 8(b) increase with wave number, and the rate of increase becomes larger as the field is increased. Note that the $\mathbf{M}$ vectors make relatively large angles with the BLS $\mathbf{k}$ vector for all fields, as for surface modes. An increase is expected for surfacelike modes. The observed behavior is qualitatively consistent with the solid lines obtained from theory. The behavior below the region (ii) jump and fields below 200 Oe is similar to the low-field easy axis results.

Figure 9 shows BLS spin-wave frequency data for the [110] uniaxial hard in-plane direction field case as in Fig. 8(b), but shown as frequency versus field for different values of the in-plane wave number k. The k values shown, 0.67×10^5, 1.48×10^5, 1.82×10^5, and 2.23×10^5 rad/cm, correspond to angles of incidence of 15°, 35°, 45°, and 65°, respectively. The data for $\theta=35°$ and $k=1.48\times10^5$ cm^{-1} are the same as in Fig. 6(b). Only the Stokes data are shown. These data are shown in a frequency versus field format to show explicitly the soft-mode behavior at $H\approx170$ Oe and at $H\approx1125$ Oe. This soft-mode behavior is particularly pronounced for the data for the lowest k value. The region (ii) flip in the $\mathbf{M}_1$ and $\mathbf{M}_2$ vectors at $H\approx170$ Oe leads to the sharp minimum evident from Fig. 6(b) and Fig. 9. The gradual collapse in the angle between $\mathbf{M}_1$ and $\mathbf{M}_2$ to zero at saturation for $H\approx1125$ Oe leads to the less-pronounced second minimum.

V. THEORY

The solid lines shown in Figs. 6 and 8 are from the theory of Stamps[30] for spin waves in sandwich films with very thin exchange-coupled magnetic layers. The purpose of this section is to summarize the elements of this theory and to discuss further the connection between the BLS data presented above and calculated spin-wave frequencies for sandwich films.

The theory follows a basic micromagnetic approach[23,33] which combines torque equations of motion for the magnetizations $\mathbf{M}_1$ and $\mathbf{M}_2$ for two thin magnetic layers, effective fields $\mathbf{H}_1$ and $\mathbf{H}_2$ which act on the $\mathbf{M}_1$ and $\mathbf{M}_2$, and appropriate boundary conditions to determine the normal modes of the system. The effective fields include terms due to the applied field $\mathbf{H}$, exchange, cubic and uniaxial anisotropy, and dipole-dipole interactions. The dipole field Fourier component $\mathbf{h}(\mathbf{k},y)$, where y denotes the coordinate perpendicular to the film plane, is related to the dynamic magnetization Fourier components $\mathbf{m}_1(\mathbf{k},y)$ and $\mathbf{m}_2(\mathbf{k},y)$ for the two layers through the Maxwell equations and a Green's function formalism.[34] This procedure yields two sets of coupled integral equations involving $\mathbf{m}_1$ and $\mathbf{m}_2$.

The solution of these coupled equations, which is quite complicated for thick magnetic films, is simplified considerably for the lowest-frequency modes and very thin magnetic layers. This simplification is due to the fact that for very thin magnetic layers, the lowest-frequency mode for a single layer is a near-uniform mode for which $\mathbf{m}_1$ or $\mathbf{m}_2$ is essentially constant across the film thickness. This, in turn, allows one to average the fields $\mathbf{H}_1$ and $\mathbf{H}_2$ over the thickness of the films and simplify the calculation considerably.[35–37] Through this averaging process, one invokes the so-called Hoffmann boundary conditions at the magnetic film surfaces.[38] The final result is a set of six coupled equations in the form

Downloaded 26 Dec 2001 to 129.82.140.114. Redistribution subject to AIP license or copyright, see http://ojps.aip.org/japo/japcr.jsp

$$\left(\mathbf{L}_{\text{op}}-\frac{\omega}{\gamma}\right)\begin{bmatrix}\mathbf{m}_1\\ \mathbf{m}_2\end{bmatrix}=0, \tag{3}$$

where $\mathbf{L}_{\text{op}}$ represents a matrix of terms containing the field H and the various magnetic parameters for the sandwich already listed in Eq. (1), ω is the spin-wave frequency, and γ denotes the gyromagnetic ratio for the material. The system of six equations represented by Eq. (3) can be solved for the normal mode spin-wave frequencies and the normal mode $\mathbf{m}_1$ or $\mathbf{m}_2$ distributions.

Finally, by properly choosing coordinate systems such that the local z_1 and z_2 axes, for example, are in the directions of the static components of the $\mathbf{M}_1$ and $\mathbf{M}_2$ vectors in the two magnetic layers, the number of coupled equations can be reduced from six to four. The solutions correspond, in certain limits, to in-phase and out-of-phase precessions for the $\mathbf{M}_1$ and $\mathbf{M}_2$ vectors. In the high-field limit with the static components of $\mathbf{M}_1$ and $\mathbf{M}_2$ parallel, the in-phase mode reduces to the usual uniform precession ferromagnetic resonance mode with the $\mathbf{M}_1$ and $\mathbf{M}_2$ precessions in phase. For the out-of-phase mode, the precessional motions for $\mathbf{M}_1$ and $\mathbf{M}_2$ in this limit are out of phase by 180°. As in the case of bulk two sublattice antiferromagnets and ferrimagnets, the in-phase and out-of-phase mode frequencies can be different. In such systems, the out-of-phase mode frequency is usually much higher than the in-phase mode frequency. For sandwich films, the out-of-phase mode frequency can be higher or lower than the in-phase mode frequency, depending on the field $\mathbf{H}$ and the static configuration for $\mathbf{M}_1$ and $\mathbf{M}_2$. The mode frequencies can also be different for opposite spin-wave propagation directions. This represents an extension of the nonreciprocal propagation property for surface modes in the Damon–Eshbach theory.

The mathematical details of the theory outlined above are presented in Ref. 30. The results presented here consist of numerical calculations of frequency versus field or wave number for the set of parameters obtained in Sec. IV in connection with the feature fits between Figs. 6 and 7, and with one additional parameter for surface anisotropy. Surface anisotropy is considered below.

In the saturated regimes of Figs. 6(a) and 6(b), one can make use of a simple analytical solution from Ref. 30 for the in-phase or acoustic mode and $\mathbf{k}$ perpendicular to $\mathbf{H}$. In this limit, the sandwich film acoustic mode spin-wave frequency to lowest order in kd is

$$\omega_a^2=\omega_B^2+\tfrac{1}{2}\gamma^2(4\pi M_s)^2(1+e^{-ks})kd, \tag{4}$$

where ω_B denotes the frequency at the top of the bulk spin-wave band or the Damon–Eshbach frequency in the limit $k=0$, s is the thickness of the intermediate nonmagnetic layer in the sandwich, and d is the nominal magnetic layer thickness. For isotropic films, this frequency is given by $\omega_B=[H(H+4\pi M_s)]^{1/2}$. Additional terms are present for anisotropic materials. In any event, when the exponential term in Eq. (3) is small, the expression reduces to the DE surface mode frequency for $\mathbf{k}$ perpendicular to $\mathbf{H}$ and $\mathbf{M}_s$ in a single layer of thickness $2d$. As indicated earlier, with $s=13$ Å and k in the 1×10^5–2×10^5 rad/cm range, the ks product is indeed small.

This small ks limit is applicable, therefore, to the region (iii) BLS data in Fig. 6(a) for $H>300$ Oe, and to the region (iv) data in Fig. 6(b) for $H>1000$–1200 Oe. The corresponding curves are shown by the lines in Figs. 6(a) and 6(b) labeled "DE," where ω_B vs H has been evaluated with the appropriate cubic and uniaxial anisotropy effective field terms taken into account. Both lines track the respective data, but are upshifted by about 1–2 GHz. Following Cochran *et al.*,[36] this discrepancy with the BLS data can be attributed to surface anisotropy. The inclusion in the theory of a surface anisotropy with the easy axis perpendicular to the magnetic layers causes a downshift in the DE frequency. This effect can be included in analyses for ferromagnetic resonance and DE theory for single-layer thin films by simply replacing the saturation induction $4\pi M_s$ by an effective saturation induction parameter $4\pi M_{\text{eff}}$ given by

$$4\pi M_{\text{eff}}=4\pi M_s-\frac{2K_s}{M_s d}, \tag{5}$$

where d represents the nominal film thickness and K_s is a uniaxial surface anisotropy energy density parameter.[36] A value of 2 kOe for $2K_s/M_s d$ pushes the DE curve in Fig. 6(a) down to match the data points. The solid lines through the data points in the saturated regions show the results from the full theory. The above value of $2K_s/M_s d$ is consistent with surface anisotropy effects observed for iron layers in Fe-Cu systems,[36] Fe-Ag, Fe-Au, Fe-Cu, and Fe-Cu systems,[39] and Fe-Mo and Fe-Pd systems.[40] In principle, one could use different corrections for the two iron layers based on different values of K_s for the different interfaces and the different thicknesses for the magnetic layers. This has not been done. The theoretical curves in Figs. 6 and 8 were obtained simply by incorporating the surface anisotropy into the Hoffmann boundary condition at the magnetic layer surfaces with a surface anisotropy field $H_s=2K_s/M_s d=2$ kOe.

Based on the above, a full set of sandwich film parameters with which to perform numerical calculations of the acoustic and optical mode frequencies for detailed comparison with the BLS data described above is now in hand. To summarize, these parameters are: saturation induction $4\pi M_s=18.6$ kG; cubic anisotropy field $H_A=550$ Oe; in-plane [110] easy axis uniaxial anisotropy field $H_U=76$ Oe; effective interlayer exchange coupling field $H_J=120$ Oe; magnetic layer thickness ratio $d_1/d_2=0.91$; gyromagnetic ratio $\gamma=2.9$ MHz/Oe; and surface anisotropy field $H_s=2$ kOe.

Results of the frequency versus field calculations are shown in Fig. 10. In the same format as Fig. 6, the curves shown in Fig. 10(a) are for the [100] direction field case and the curves in Fig. 10(b) are for the [110] uniaxial hard in-plane direction field case. Each graph contains four curves. For clarity, symbols rather than lines are used to show the results. The "I" and "O" labels indicate the in-phase and the out-of-phase mode frequencies, respectively.

Downloaded 26 Dec 2001 to 129.82.140.114. Redistribution subject to AIP license or copyright, see http://ojps.aip.org/japo/japcr.jsp

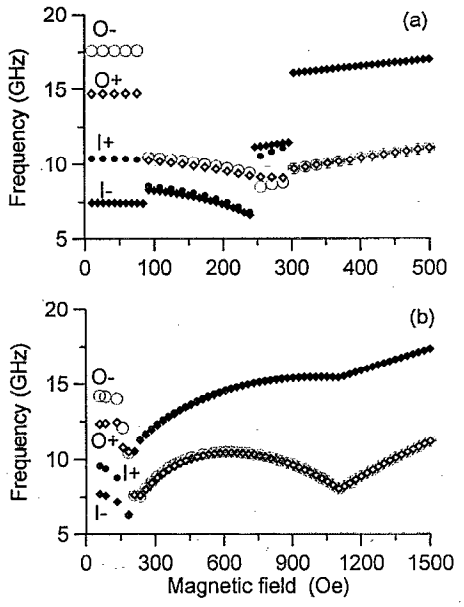

FIG. 10. Calculated spin-wave frequency vs field for the Fe/Cr/Fe sandwich film with (a) an in-plane [100] direction field and (b) a [110] uniaxial hard in-plane direction field. The in-plane spin-wave wave vector k was perpendicular to the field and the wave number was 1.48×10^5 rad/cm. The circle and diamond symbols designate opposite directions of k. The solid and open symbols designate the in-phase and out-of-phase mode frequencies, respectively.

The + and − labels indicate opposite directions for the in-plane wave vector k. The k vectors were perpendicular to the field **H**, as in the experiments. The wave number for the calculations was the same as for Fig. 6, $k=1.48\times10^5$ rad/cm.

There are clear correlations between the data in Fig. 6 and the calculations. First, all of the frequency jumps match the data. This is to be expected on the basis of the magnetization curve matchups already discussed. Second, with one exception, the calculations indicate an overall match between the calculated in-phase mode frequencies and the measured frequencies for both [100] and [110] direction fields. The exception is for the [100] field direction plateau region. Here, the frequency matchup appears to be for the out-of-phase mode. The solid lines in Fig. 6 show the selected curves from Fig. 10 which match up with the data.

The large splitting between the + and − in-phase modes at low field for both the [100] and the [110] field directions closely match the observed S and AS frequency differences in these same field regimes. The mode propagation characteristics in these field ranges are clearly nonreciprocal. The calculations show, moreover, that the both the I and O modes are nonreciprocal whenever the $\mathbf{M}_1$ and $\mathbf{M}_2$ vectors are not strictly parallel. These results demonstrate the extension of the nonreciprocal Damon–Eshbach surface mode property to magnetic sandwiches.[12] The observed matchups between the data and the calculated in-phase mode frequencies, and the absence of experimental BLS peaks for out-of-phase modes, is consistent with basic scattering considerations.[41] The 9% difference in thickness between the magnetic layers is insufficient to give enough signal for the out-of-phase modes to be observed.

The solid lines in Fig. 8 show calculated in-phase mode frequencies versus wave number k for the applicable field directions and field values which correspond to the measurements. These curves show quantitative agreement for the [100] direction and qualitative agreement for the [110] direction.

VI. SUMMARY AND CONCLUSION

The technique of Brillouin light scattering has been used to examine in detail the field and wave-number dependencies of the low-wave-number spin-wave frequencies for in-plane magnetized Fe/Cr/Fe sandwich films. The BLS technique is able to resolve critical features in the response which are not evident from magnetization curves. These features include, in the case of an easy direction [100] applied field, (i) a distinct splitting between the Stokes and anti-Stokes signals at low field and (ii) a plateau in the response associated with the jump between nearly antiparallel alignment of the iron layer magnetizations at low field and the nearly parallel alignment of these magnetizations at high field. These two features can be modeled quantitatively in terms of a difference in thickness for the iron layers and an in-plane [110] uniaxial anisotropy. A careful match between the features of calculated magnetization curves and the BLS data gives accurate values of the magnetic parameters for the sandwich and the thickness ratio for the iron layers. Calculations of spin-wave frequencies from the theory of Stamps have also been made and compared to the measured frequencies. One additional parameter for surface anisotropy was introduced to match the calculated in-phase mode frequency for the sandwich film Damon–Eshbach mode to the data. Quantitative agreement between the theory and the data was found.

ACKNOWLEDGMENTS

Dr. J. J. Krebs of the Naval Research Laboratories, Washington, DC, is acknowledged for providing the Fe/Cr/Fe thin films used in this work, for the measurements shown in Fig. 1, and for helpful comments and discussions on the results. Professor J. F. Cochran, Simon Fraser University, Burnaby, British Columbia, Canada, is gratefully acknowledged for providing an advance copy of his unpublished review article on light scattering from ultrathin magnetic layers and bilayers. This work was supported in part by the National Science Foundation, Grant No. DMR-8921761, by the U.S. Army Research Office, Grant No. DAAL03-91-G-0327, and the Office of Naval Research, Grant No. N00014-90-J-4078.

[1] M. N. Baibich, J. M. Broto, A. Fert, F. Nguyen Van Dau, F. Petroff, P. Eitenne, G. Creuzet, A. Friederich, and J. Chazelas, Phys. Rev. Lett. **61**, 2472 (1988).
[2] P. Grünberg, J. Barnas, F. Saurenbach, J. A. Fuss, A. Wolf, and M. Vohl, J. Magn. Magn. Mater. **93**, 58 (1991).
[3] A. Fert, A. Barthélémy, P. Etienne, S. Lequien, R. Loloee, D. K. Lottis, D. H. Mosca, F. Petroff, W. P. Pratt, and P. A. Schroeder, J. Magn. Magn. Mater. **104-107**, 1712 (1992).

Downloaded 26 Dec 2001 to 129.82.140.114. Redistribution subject to AIP license or copyright, see http://ojps.aip.org/japo/japcr.jsp

[4] J. R. Sandercock, in *Light Scattering in Solids III, Recent Results*, edited by M. Cardona and G. Güntherodt (Springer, Berlin, 1982), pp. 173–206.
[5] C. E. Patton, Phys. Rep. **103**, 251 (1984).
[6] P. Grünberg and K. Mika, Phys. Rev. B **27**, 2955 (1983).
[7] M. Grimsditch, M. R. Khan, A. Kueny, and I. K. Schuller, Phys. Rev. Lett. **51**, 498 (1983).
[8] I. K. Schuller and M. Grimsditch, J. Appl. Phys. **55**, 2491 (1984).
[9] A. Kueny, M. R. Khan, I. K. Schuller, and M. Grimsditch, Phys. Rev. B **29**, 2879 (1984).
[10] G. Rupp, W. Wettling, and W. Jantz, Appl. Phys. A **37**, 73 (1985).
[11] P. A. Grünberg, Prog. Surf. Sci. **18**, 1 (1985).
[12] P. Grünberg, J. Appl. Phys. **57**, 3673 (1985).
[13] B. Hillebrands, P. Baumgart, R. Mock, G. Güntherodt, A. Boufelfel, and C. M. Falco, Phys. Rev. B **34**, 9000 (1986).
[14] R. E. Camley, Surf. Sci. Rep. **7**, 103 (1987).
[15] J. R. Dutcher, B. Heinrich, J. F. Cochran, D. A. Steigerwald, and W. F. Egelhoff, Jr., J. Appl. Phys. **63**, 3464 (1988).
[16] B. Hillebrands, A. Boufelfel, C. M. Falco, P. Baumgart, G. Güntherodt, E. Zirngiebl, and J. D. Thompson, J. Appl. Phys. **63**, 3880 (1988).
[17] M. H. Grimsditch, in *Light Scattering in Solids V*, edited by M. Cardona and G. Güntherodt, *Topics in Applied Physics*, Vol. 66 (Springer, Berlin, 1989), Chap. 7.
[18] P. Grünberg, in *Light Scattering in Solids V*, edited by M. Cardona and G. Güntherodt, *Topics in Applied Physics*, Vol. 66 (Springer, Berlin, 1989), Chap. 8.
[19] J. F. Cochran, J. Rudd, W. B. Muir, B. Heinrich, and Z. Celinski, Phys. Rev. B **42**, 508 (1990).
[20] P. Grünberg, R. Schreiber, Y. Pang, M. B. Brodsky, and H. Sowers, Phys. Rev. Lett. **57**, 2442 (1986).
[21] P. Grünberg, R. Schreiber, Y. Pang, U. Walz, M. B. Brodsky, and H. Sowers, J. Appl. Phys. **61**, 3750 (1987).
[22] F. Saurenbach, U. Walz, L. Hinchey, P. Grünberg, and W. Zinn, J. Appl. Phys. **63**, 3473 (1988).
[23] J. Barnas and P. Grünberg, J. Magn. Magn. Mater. **82**, 186 (1989).
[24] M. Vohl, J. Barnas, and P. Grünberg, Phys. Rev. B **39**, 12 003 (1989).
[25] S. Demokritov, J. A. Wolf, and P. Grünberg, Europhys. Lett. **15**, 881 (1991).
[26] P. Grünberg, S. Demokritov, A. Fuss, M. Vohl, and J. A. Wolf, J. Appl. Phys. **69**, 4789 (1991).
[27] J. J. Krebs, P. Lubitz, A. Chaiken, and G. A. Prinz, J. Appl. Phys. **67**, 5920 (1990).
[28] R. W. Damon and J. R. Eshbach, J. Phys. Chem. Solids **19**, 308 (1961).
[29] See, for example, Circuits Systems and Signal Processing **4**, 5–363 (1985) [special issue, "Magnetostatic Waves and Applications to Signal Processing"].
[30] R. L. Stamps, Phys. Rev. B **49**, 339 (1994).
[31] Interferometer system manufactured by JRS, Ltd., Zwillikerstrasse 8, 8910 Affoltern a. A., Switzerland.
[32] J. R. Sandercock and W. Wettling, J. Appl. Phys. **50**, 7784 (1979).
[33] B. Hillebrands, Phys. Rev. B **41**, 530 (1990).
[34] See, for example, T. S. Rahman and D. L. Mills, Phys. Rev. B **20**, 1173 (1979); B. A. Kalinikos and A. N. Slavin, J. Phys. C **19**, 7013 (1986); Acta Phys. Polon. A **75**, 541 (1989).
[35] B. Heinrich, S. T. Purcell, J. R. Dutcher, K. B. Urquhart, J. F. Cochran, and A. S. Arrott, Phys. Rev. B **38**, 12879 (1988).
[36] J. F. Cochran, J. Rudd, W. B. Muir, B. Heinrich, and Z. Celinski, Phys. Rev. B **42**, 508 (1990).
[37] R. L. Stamps and B. Hillebrands, Phys. Rev. B **44**, 12 417 (1991).
[38] F. Hoffmann, Phys. Status Solidi **41**, 807 (1970); F. Hoffmann, A. Stankoff, and H. Pascard, J. Appl. Phys. **41**, 1022 (1970).
[39] B. Heinrich, Z. Celinski, J. F. Cochran, A. S. Arrott, and K. Myrtle, J. Appl. Phys. **70**, 5769 (1991).
[40] Y. Obi, Y. Kawano, Y. Tange, and H. Fujimori, J. Magn. Mag. Mater. **93**, 587 (1991).
[41] J. F. Cochran and J. R. Dutcher, J. Appl. Phys. **64**, 6092 (1988).

Downloaded 26 Dec 2001 to 129.82.140.114. Redistribution subject to AIP license or copyright, see http://ojps.aip.org/japo/japcr.jsp